analytical chemistry

pubs.acs.org/ac Article

Label-Free Immunoassay for Sensitive and Rapid Detection of the SARS-CoV-2 Antigen Based on Functionalized Magnetic Nanobeads with Chemiluminescence and Immunoactivity

Shanshan Wang, Jiangnan Shu, Aihua Lyu, Xiaoxue Huang, Weihong Zeng, Tengchuan Jin,* and Hua Cui*

Cite This: *Anal. Chem.* 2021, 93, 14238−14246 Read Online

ACCESS | Metrics & More | Article Recommendations | Supporting Information

ABSTRACT: Direct detection of SARS-CoV-2 in biological specimens is often challenging due to the low abundance of viral components and lack of enough sensitivity. Herein, we developed a new type of chemiluminescent functionalized magnetic nanomaterial for sensitive detection of the SARS-CoV-2 antigen. First, $HAuCl_4$ was reduced by *N*-(aminobutyl)-*N*-(ethylisoluminol) (ABEI) in the presence of amino magnetic beads (MB-NH_2) to generate ABEI-AuNPs, which were directly assembled on the surface of MB-NH_2. Then, Co^{2+} was modified onto the surface to form MB@ABEI-Au/Co^{2+} (MAA/Co^{2+}). MAA/Co^{2+} exhibited good chemiluminescence (CL) and magnetic properties. It was also found that it was easy for the antibody to be connected with MAA/Co^{2+}. Accordingly, MAA/Co^{2+} was used as a sensing interface to construct a label-free immunoassay for rapid detection of the N protein in SARS-CoV-2. The immunoassay showed a linear range from 0.1 pg/mL to 10 ng/mL and a low detection limit of 69 fg/mL, which was superior to previously reported methods for N protein detection. It also demonstrated good selectivity by virtue of magnetic separation, which effectively removed a sample matrix after immunoreactions. It was successfully applied for the detection of the N protein in spiked human serum and saliva samples. Furthermore, the immunoassay was integrated with an automatic CL analyzer with magnetic separation to detect the N protein in patient serums and rehabilitation patient serums with satisfactory results. Thus, the CL immunoassay without a complicated labeling procedure is sensitive, selective, fast, simple, and cost-effective, which may be used to combat the COVID-19 pandemic. Finally, the CL quenching mechanism of the N protein in the immunoassay was also explored.

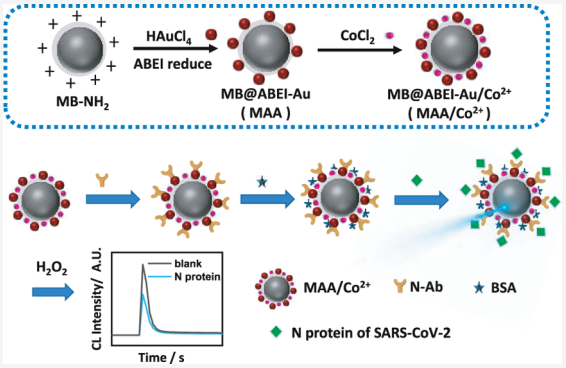

Coronavirus disease 2019 (COVID-19) is a highly transmissible severe acute respiratory syndrome that can be transmitted from person to person caused by severe acute respiratory syndrome coronavirus 2 (SARS-CoV-2), evolving into a worldwide pandemic.[1−3] Although more than a year has passed, the situation has not been improved, and mutant viruses are arising all over the world including the U.K. and South Africa.[4] The symptoms of COVID-19 are mainly acute respiratory distress syndrome, which leads to respiratory infections, resulting in varying degrees of multiple organ failure and even death. The incubation period of COVID-19 ranges from 1 to 14 days, and many asymptomatic infections are observed. Consequently, there is an emergency need to develop fast, accurate, and sensitive detection methods to quickly identify the infected people. This will not only prevent the widespread transmission of infections but also provide patients with a more valuable treatment time.

The existing SARS-CoV-2 detection methods include nucleic acid detection, antibody testing, and antigen testing.[5−11] First of all, nucleic acid detection is a highly sensitive and selective detection method. Real-time reverse transcription-polymerase chain reaction (RT-PCR) assays based on nucleic acids have been utilized as a golden standard for SARS-CoV-2 detection globally. However, nucleic acid testing is complex and costly and requires a minimum of 2 h to follow the steps of RNA extraction, reverse transcription, gene amplification, and data analysis. Furthermore, professional technicians operating in biosafety laboratories are required. Most importantly, there are about 30−40% of false-negative results in nucleic acid detection caused by improper swab sample collection and low viral dosage in the upper respiratory tract in the late stage of infection.[12] The second method is antibody detection. A number of simple and low-cost immunoassays for antibody detection were developed.[6,13,14]

Received: July 29, 2021
Accepted: October 4, 2021
Published: October 12, 2021

https://doi.org/10.1021/acs.analchem.1c03208
Anal. Chem. 2021, 93, 14238−14246

However, antibodies are generated 7−15 days after the human body is exposed to the virus. Thus, antibody testing is not suitable for early screening and diagnosis of COVID-19.[15−17] The third method is antigen detection, which has the advantages of accurate and low requirements for equipment and personnel. The structural proteins of SARS-CoV-2 include spike (S), nucleocapsid (N), envelope (E), and membrane (M) proteins. Among them, the S protein exists on the surface of virus particles, which is closely related to the infection ability and pathogenesis of COVID-19.[18] The N protein not only plays a major role in the synthesis and translation steps of SARS-CoV-2 RNA but also has a high concentration in serum, which can be detectable even after just one day of infection.[19] Furthermore, we found that the N protein has higher immunogenicity compared to that of the receptor-binding domain (RBD) of the S protein,[20] which provides higher sensitivity when it is used as a target protein. Consequently, the N protein is suitable to be the target protein for the early detection of COVID-19.[19] To date, most of the published detection methods for the N protein are immunoassays based on labeling methods, such as molecular labeling and nanomaterial labeling. For example, Yan's group prepared a Co-Fe@hemin-peroxidase nanozyme to label antibodies to construct a chemiluminescence (CL) paper assay for the detection of the S protein with a detection limit of 0.1 ng/mL.[7] He's group used the fluorescence microsphere labeling method to construct a sandwich immunosensor for the N protein based on immunochromatographic technology with a detection limit of 100 ng/mL.[9] However, immunoassays based on labeling technology require two antibodies and several steps for incubation and washing, which have disadvantages of high cost, time-consuming, complicated operation, and are difficult to meet the needs of rapid clinical diagnosis.

In recent years, label-free methodologies with various detection techniques for quantitative analysis of targets based on signal changes caused by the specific binding of antigens and antibodies have attracted much attention.[21] Compared with labeled methods, label-free immunoassays have the advantages of fast speed, low cost, and high simplicity. Among the detection technologies, CL has the advantages of high sensitivity, wide linear range, low cost, and uncomplicated manipulation, which lead to a wide application in many fields. CL-functionalized materials such as CL-functionalized carbon nanomaterials,[22] metal nanomaterials,[23] quantum dots,[24] metal−organic frameworks,[25] and magnetic materials[25−27] are often used as the sensing interfaces for label-free immunoassays to achieve high-sensitivity detection. Among them, CL-functionalized magnetic beads (MBs) with good magnetic and CL properties have attracted much attention. Several CL-functionalized MBs have been synthesized such as Co^{2+}/*N*-(aminobutyl)-*N*-(ethylisoluminol) (ABEI)-functionalized MBs (Co^{2+}/ABEI/MBs)[28] and Co^{2+}/ABEI-functionalized magnetic carbon composite (Co^{2+}/ABEI-Fe_3O_4@void@C).[29] On the one hand, MBs with a large specific surface area and abundant functional groups can connect a number of signal molecules and antibodies to realize target sensing. On the other hand, the immunocomplex can be directly separated to remove the interferents from a sample matrix after immunoreactions. However, complicated procedures are needed for the connection of antibodies on the surface of MBs. For example, it was difficult to attach antibodies on the surface of Co^{2+}/ABEI/MBs.[28] While in the construction of the immunoassay based on Co^{2+}/ABEI-Fe_3O_4@void@C,[29] chitosan was first assembled, and then the AuNP-functionalized antibody was synthesized and combined onto the CL-functionalized MBs through electrostatic adsorption and the covalent Au−N bond. Furthermore, there are a few reports on the detection of COVID-19 using the label-free methodologies. Therefore, it is important and necessary to develop accurate, sensitive, and rapid label-free immunoassays for SARS-CoV-2 antigen detection.

In this work, a facile strategy was developed for the synthesis of CL-functionalized magnetic materials MB@ABEI-Au/Co^{2+} (MAA/Co^{2+}) by reducing $HAuCl_4$ with ABEI to form ABEI-AuNPs in situ on the surface of MB-NH_2 and combining cobalt ions via electrostatic adsorption and coordination reaction. MAA/Co^{2+} was characterized by transmission electron microscopy (TEM), ζ potential, X-ray photoelectron spectroscopy (XPS), inductively coupled plasma mass spectrometry (ICP-MS), and saturation magnetization. The CL behavior and mechanism of MAA/Co^{2+} were studied. Moreover, it was found that the antibody could directly connect to AuNPs in MAA/Co^{2+} through the Au−N bond, Au−S bond, and electrostatic adsorption, and thus, a label-free immunoassay for detecting the N protein of SARS-CoV-2 was constructed. After condition optimization in each step, the sensitivity, selectivity, and stability of the proposed immunoassay were investigated. The applicability of the immunoassays in real human serum was examined. Finally, the CL quenching mechanism of the protein and antigen in the immunoassay was also studied.

EXPERIMENTAL SECTION

Chemicals and Materials. All chemicals and materials used in this work are described in the Supporting Information.

Synthesis of MAA/Co^{2+}. MAA/Co^{2+} was synthesized through a two-step method. The first step is the synthesis of MAA. First, 1 mg of MB-NH_2 was washed twice with ethanol and dispersed in 0.5 mL of ethanol solution. Then, 1.5 mL of 5 mM $HAuCl_4$ was added to obtain a mixture. After adding 0.5 mL of 4 mM ABEI (pH 13.0) to the above solution under shaking and vigorous stirring for 2 h, the mixture was moved onto a vertical mixer to continue the reaction overnight at room temperature. Finally, the synthesized MAA was washed twice with ultrapure water, dispersed in 1 mL of ultrapure water, and stored at 4 °C for further use.[30,31]

The second step is to combine cobalt ions with MAA. To obtain MAA/Co^{2+}, 0.1 mL of 5 mM Co^{2+} aqueous solution was added to 1 mL of MAA and stirred at room temperature for 3 h. Then, the resulting suspension was magnetically separated, washed twice, and dispersed in 1 mL of water. Finally, MAA/Co^{2+} was obtained and stored at 4 °C.

Characterization of MAA/Co^{2+}. TEM images were taken from a Talos F200X electronic microscope (FEI). The concentrations of Co^{2+} in MAA/Co^{2+} were obtained by the ICP-AES measurement carried out on an Optima 7300 DV plasma atomic emission spectrometer (PerkinElmer). XPS was measured by a Thermo ESCALAB 250Xi electron spectrograph (VG Scientific, East Grinstead, U.K.) with Al Kα radiation as the X-ray source. The ζ potential values of synthesized nanomaterials and dynamic light scattering intensities of the immunoassay were obtained by a ζ potential analyzer (Nano ZS90 Zetasizer, Malvern Instruments, Malvern, U.K.). Magnetic hysteresis curves of MAA/Co^{2+} were obtained using a vibrating sample magnetometer (Quantum Design Inc.). The free radicals involved in the CL

https://doi.org/10.1021/acs.analchem.1c03208
Anal. Chem. 2021, 93, 14238−14246

Scheme 1. Schematic Illustration for the Synthesis of MAA/Co^{2+} and Fabrication Procedures of Label-Free CL Immunoassay for the Detection of the N Protein

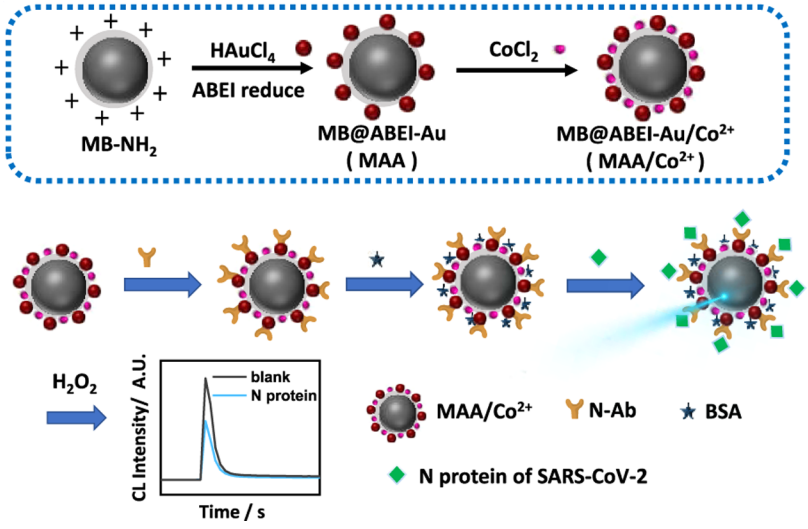

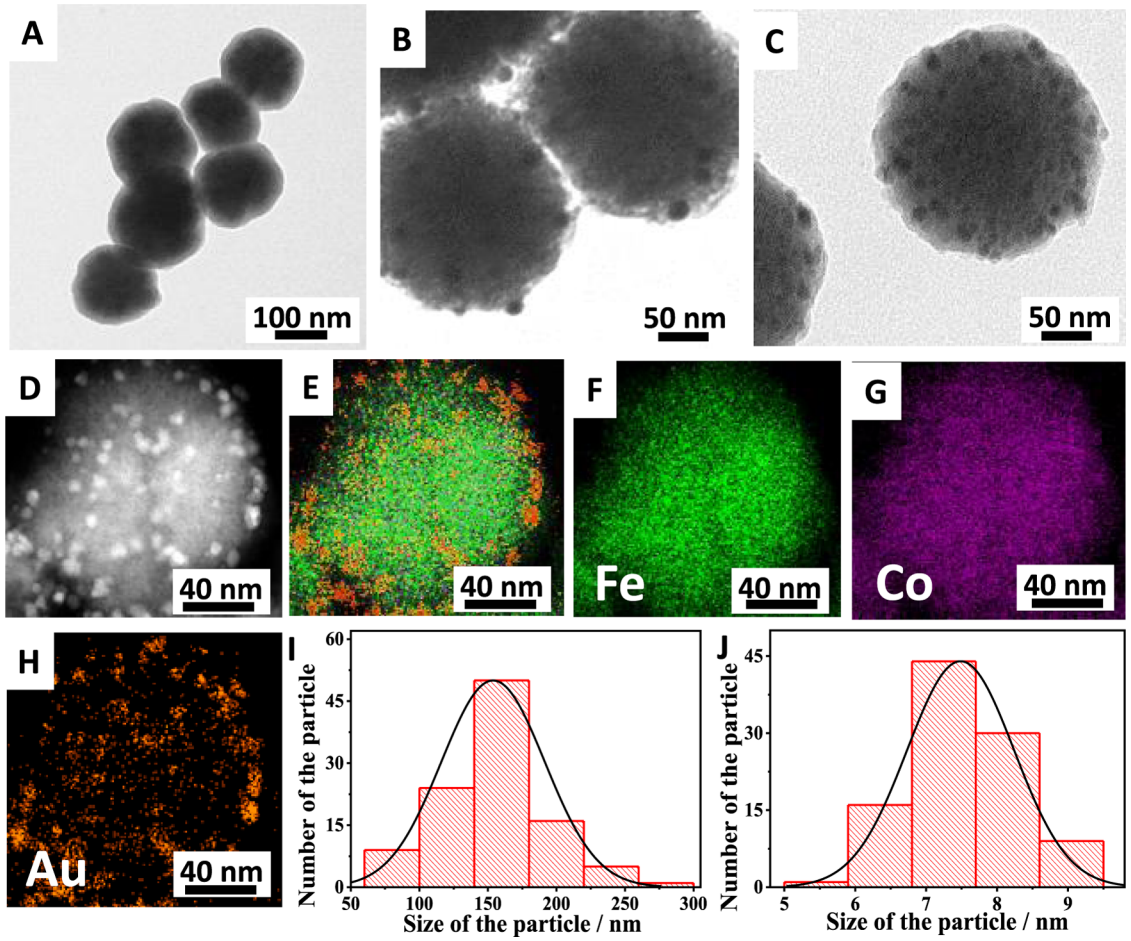

Figure 1. TEM images of (A) MB-NH_2, (B) MAA, and (C) MAA/Co^{2+}. (D–H) TEM image and elemental mapping analyses of a single MAA/Co^{2+} particle. The histogram of the size distribution of (I) MB-NH_2 and (J) AuNPs in MAA/Co^{2+}.

reaction of MAA/Co^{2+} with H_2O_2 were characterized by electron spin resonance (ESR) spectra (JES-FA200, JEOL, Japan). CL was measured with a Centro LB960 microplate luminometer (Berthold, Germany). Clinical samples were determined with an automatic CL analyzer with a magnetic separation function (Kaeser 1000, Kangrun Biotech, China).

CL Measurements. In a typical assay, 50 μL of MAA/Co^{2+} was added into each well of a 96-well microplate, and then 50 μL of 0.01 M NaOH (pH 12.0) containing 1 mM H_2O_2 solution was injected into each well. CL kinetic curves were recorded using a microplate luminometer when injecting H_2O_2

https://doi.org/10.1021/acs.analchem.1c03208
Anal. Chem. 2021, 93, 14238−14246

solution. The measurement time was optimized as 10 s with a time interval of 0.1 s.

Fabrication of CL Immunoassay for the N protein. For the construction of label-free immunoassays, the procedures are shown in Scheme 1. First, 25 μL of 1 mg/mL rabbit anti-N protein polyclonal antibody (N-Ab) was added to 1 mL of MAA/Co^{2+} and reacted for 0.5 h at room temperature. After magnetic separation and washing with 0.01 M phosphate-buffered saline (PBS) buffer (pH 7.4), MAA/Co^{2+}/N-Ab was dispersed in 1% bovine serum albumin (BSA) solution for blocking and reacted for another 0.5 h. Next, the obtained MAA/Co^{2+}/N-Ab/BSA was separated magnetically, washed with PBS, dissolved in 1.5 mL of PBS, and stored at 4 °C. For the CL detection of the N protein, 200 μL of the N protein with different concentrations (1.0×10^{-8} to 1.0×10^{-13} g/mL) was incubated with 200 μL of MAA/Co^{2+}/N-Ab/BSA suspension under gentle shaking at 37 °C for 20 min, followed by washing via magnetic separation and dispersing in 200 μL of PBS solution.

Afterward, 50 μL of H_2O_2 (pH 12.0) was injected into each well of a 96-well plate with 50 μL of the as-prepared MAA/Co^{2+}/N-Ab/BSA/N protein, and the CL kinetic curves of each well were recorded at the same time.

RESULTS AND DISCUSSION

Synthesis and Characterization of MAA/Co^{2+}. The synthesis of MAA/Co^{2+} is illustrated in Scheme 1. $HAuCl_4$ was first reduced by ABEI in the presence of MB-NH_2 to form ABEI-AuNPs in situ, which were adsorbed onto the surface of MB-NH_2 by the Au−N covalent interaction.[31] After being combined with Co^{2+} by electrostatic adsorption and the coordination reaction, MAA/Co^{2+} was obtained subsequently.

To confirm the successful synthesis of MAA/Co^{2+}, TEM, XPS, ζ potential, ICP-MS, and saturation magnetization were used for the characterization of nanomaterials. The size and morphology of nanomaterials were characterized via TEM images as shown in Figure 1. First, MB-NH_2 exhibited a spherical structure with a very smooth surface, and the diameter was approximately 100−200 nm as shown in Figure 1A,I. After reducing $HAuCl_4$ with ABEI in situ on MB-NH_2, the formed ABEI-AuNPs were obviously well-dispersed on the surface of MB-NH_2 and the particle diameter of ABEI-AuNPs was about 7−8 nm as shown in Figure 1B,J, which indicated the successful synthesis of MAA. After being combined with Co^{2+}, the morphology of MAA/Co^{2+} is shown in Figure 1C,D. Although there is no obvious change in the morphology of MAA/Co^{2+} after Co^{2+} loading, element mapping images in Figure 1E−H show Co^{2+} on the surface of MAA and the successful synthesis of MAA/Co^{2+}.

In addition, the XPS spectra of MAA and MAA/Co^{2+} are shown in Figures S1 and S2. To begin with, the Au 4f spectrum of MAA/Co^{2+} was curve-fitted into the doublet components for Au $4f_{7/2}$ and Au $4f_{5/2}$ in Figure S2A, which supported the presence of Au^0. Then, the N 1s spectrum at 398.4 and 401.8 eV of MAA/Co^{2+} in Figure S1B and S2B was attributed to the nitrogen atoms in the −N−C− and NH−C═O groups, indicating that ABEI molecules were present on the surface of as-prepared nanomaterials. The peak at 288.75 eV of C 1s in Figure S2C corresponding to the presence of the −COOH group on the surface of MAA/Co^{2+} confirmed the presence of oxidation products of ABEI. Simultaneously, the XPS survey of MAA/Co^{2+} at a peak around 780 eV in Figure S2D was attributed to Co 2p, indicating the presence of Co^{2+} in MAA/Co^{2+}. These results demonstrated that Co could be combined onto MAA by a coordination reaction and MAA/Co^{2+} was well prepared.

Besides, the successful combination of Co^{2+} was also verified by the ζ potential and ICP-MS. ICP-MS indicated that the concentration of the Co element on MAA/Co^{2+} was 47.2 ng/mL. As shown in Figure S3, the measured ζ potentials of MB-NH_2, MAA, and MAA/Co^{2+} in aqueous solution were 9.89, −23.32, and −9.23 mV, respectively. The immobilization of ABEI-Au decreased the ζ potential of the positively charged MB-NH_2, leading to the generation of a negatively charged complex. After the assembly of Co^{2+}, the ζ potential of MAA/Co^{2+} was positively shifted by 14.10 mV, which indicated that Co^{2+} could also be captured on the negatively charged MAA via electrostatic interaction. Moreover, the saturation magnetization of MAA/Co^{2+} was 55.98 emu/g as shown in Figure 2A,

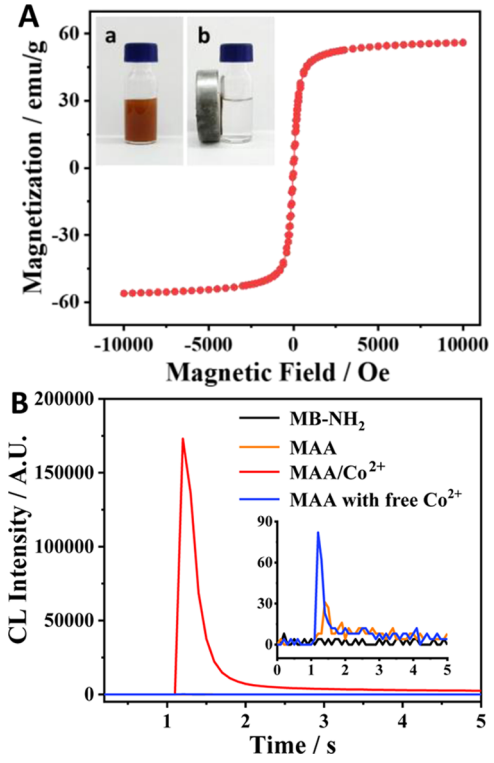

Figure 2. (A) Magnetic hysteresis curves of MAA/Co^{2+}. Inset: Photographs of MAA/Co^{2+} (a) before and (b) after applying an external magnetic field. (B) CL kinetics curves of MB-NH_2, MAA, MAA/Co^{2+}, and MAA with free Co^{2+}. Reaction conditions: 0.1 M H_2O_2 (pH 12.0).

which met the requirement of magnetic separation. The photograph of MAA/Co^{2+} under an external magnetic field as shown in the inset of Figure 2A also confirmed that it could be completely separated under an external magnetic field. Hence, the results indicated that the CL-functionalized magnetic material MAA/Co^{2+} was successfully prepared.

CL Properties of MAA/Co^{2+}. The CL properties of the as-prepared MAA/Co^{2+} were explored by static injection on a microplate luminometer. It has been reported that metal ions, especially Co^{2+}, could strongly catalyze the CL reaction between ABEI and H_2O_2;[32,33] thus, the concentration of Co^{2+} in MAA/Co^{2+} was optimized from 0.1 to 100 mM. As shown in Figure S4, when the concentration was lower than 5 mM, the CL intensity increased with increasing the

https://doi.org/10.1021/acs.analchem.1c03208
Anal. Chem. 2021, 93, 14238−14246

concentration of Co^{2+}. When the concentration further increased, the CL signals decreased because a higher concentration of Co^{2+} would result in particle agglomeration and poor dispersion. Thus, the highest CL signal was obtained when the concentration of Co^{2+} was 5 mM.

To better understand the superior CL performance of MAA/Co^{2+}, the intensities of MB-NH_2 and MAA were tested as controls. As shown in Figure 2B, MB-NH_2 had no CL activity (black curve) and MAA showed very weak CL intensity at around 30 au (orange curve). After being incubated with 5 mM $CoCl_2$ solution, the CL intensity of MAA/Co^{2+} (red curve) was increased to 175 000 au, which was 5766 times higher than that of MAA in the same conditions. In comparison, free Co^{2+} with the same concentration as Co^{2+} on the surface of MAA/Co^{2+} was added to the solution of MAA. As shown in the blue curve of Figure 2B inset, the CL intensity of MAA with free Co^{2+} increased by only about three times compared with MAA and was 1944 times weaker than the intensity of MAA/Co^{2+}. The results indicated that the CL activity of Co^{2+}-functionalized MAA was much better than that of MAA with free Co^{2+} in the solution. The possible reason was that Co^{2+} was highly concentrated on the surface of MAA, which might be much higher than the actual content in the bulk solution, and thus, it could quickly and massively catalyze nearby H_2O_2 and then react with ABEI on the surface of MAA, resulting in stronger CL emission to some extent. In addition, a large number of carboxyl groups in the oxidation products of ABEI and amino groups on the surface of MB-NH_2 in MAA could chelate with Co^{2+} to form a stable complex, which possessed higher catalytic efficiency than Co^{2+} in aqueous solution.[34] Thus, the as-synthesized MAA/Co^{2+} has outstanding CL performance. The CL performance is attributed to the high catalytic efficiency of Co^{2+} and AuNPs and the facilitation of AuNPs for radical generation and electron transfer,[32] which is described in the Supporting Information (the proposed CL mechanism, Figure S5).

Label-Free Strategy for CL Immunoassay. Considering the excellent CL property, MAA/Co^{2+} was further used to construct a label-free CL immunoassay for the detection of the N protein. The preparation steps are schematically illustrated in Scheme 1. AuNPs in MB@ABEI-Au/Co^{2+} played important roles. First, AuNPs could catalyze the reaction of ABEI-H_2O_2 and improve the CL performance. Second, AuNPs were used as carriers to load more luminescence and acted as a bridge connecting MBs and ABEI. Furthermore, AuNPs with good biocompatibility could be directly connected to antibodies through Au−N and Au−S bonds and hydrophobic interactions, which provided convenience for the construction of the immunosensing platform. In this case, the N protein antibody was directly conjugated onto the surface of MAA/Co^{2+} to form MAA/Co^{2+}/N-Ab.[29,35] BSA was used to block nonspecific binding sites to form MAA/Co^{2+}/N-Ab/BSA, which could be used to detect the N protein. At each step, the protein was washed with PBS solution by magnetic separation. Finally, every step of the construction of the immunoassay was characterized by CL intensity and ζ potential. Figure 3A displays the CL signal of the fabrication procedure of the immunoassay. When N-Ab, BSA, and the N protein were assembled on the surface of MAA/Co^{2+} nanocomposites successively, the CL intensity decreased gradually. The assembled procedure on the surface of MAA/Co^{2+} was also confirmed by ζ potential, as shown in Figure 3B; the ζ potential of each step decreased due to the assembly of

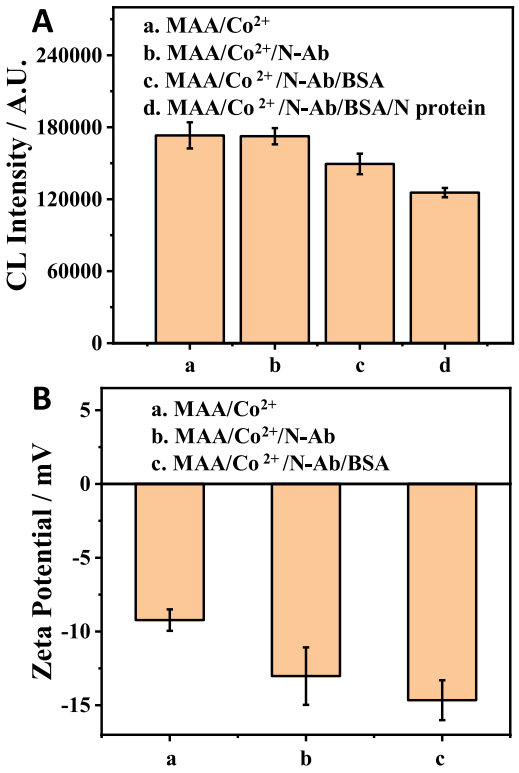

Figure 3. (A) CL signals of the immunoassay at different steps: (a) MAA/Co^{2+}, (b) MAA/Co^{2+}/N-Ab, (c) MAA/Co^{2+}/N-Ab/BSA, and (d) MAA/Co^{2+}/N-Ab/BSA/N protein. (B) ζ potential values of (a) MAA/Co^{2+}, (b) MAA/Co^{2+}/N-Ab, and (c) MAA/Co^{2+}/N-Ab/BSA.

negatively charged N-Ab and BSA, indicating successful fabrication of the label-free immunoassay.

Optimization of Experimental Conditions. Since the coverage of AuNPs on the surface of MB may affect the amount of the attached antibodies, the coverage of AuNPs on the surface of MB was optimized. The MAA with different coverage of AuNPs on the surface of MB was synthesized by reacting at different vortex mixing speeds. The corresponding CL intensity and TEM images are shown in Figure S6. With increasing the vortex mixing speed, the collision frequency and reaction probability of MBs, $HAuCl_4$, and ABEI increased, which increased the coverage of ABEI-reduced AuNPs, leading to an increase in the CL intensity of MAA/Co^{2+}. As shown in Figures 1 and S6a, the coverage of ABEI-reduced AuNPs and the CL intensity reached a maximum using a maximal vortex mixing speed, which was used for the immunosensor construction with the best analytical performance in this work. Furthermore, to investigate the CL performance of the immunoassay, the following parameters were also optimized, including the pH of H_2O_2 solution, the concentration of H_2O_2, and the incubation time of the N protein. As reported in the literature studies,[34,36] the pH value was a crucial factor influencing the CL intensity. Thus, the pH of the reaction solution was optimized between 8.0 and 13.0 by adjusting the concentration of NaOH from 1 μM to 0.1 M. As seen in Figure S7A, the highest CL intensity was achieved at pH 12.0 with 0.01 M NaOH. The proper pH could promote the decomposition of H_2O_2 into free-radical intermediates, thereby enhancing CL intensity. The concentration of H_2O_2 was optimized over the range of 0.01 to 100 mM in Figure S7B, and the maximum CL intensity was obtained when the H_2O_2

https://doi.org/10.1021/acs.analchem.1c03208
Anal. Chem. 2021, 93, 14238−14246

concentration was 1 mM. The incubation time for the immunoreaction between the antigen and antibody was also investigated using 1 ng/mL N protein. As shown in Figure S7C, the CL responses for the N protein decreased with a prolonged incubation time from 5 to 20 min and achieved constant values at 20 min, suggesting that the immunoreaction reached an equilibrium state between MAA/Co^{2+}/N-Ab/BSA and the N protein. Thus, 20 min was chosen as the optimal incubation time for the immunoassay. Consequently, a strong CL emission signal was obtained at the following conditions: 1 mM H_2O_2 containing 0.01 M NaOH (pH 12.0) and incubation of the N protein for 20 min.

Performance of CL Immunoassay for N Protein Detection. Under optimized conditions, the analytical performance of the as-prepared CL immunoassay for the determination of the N protein was investigated. As shown in Figure 4A, a gradual CL decrease was observed with the increasing concentration of the N protein. A good linear correlation between the CL response and the logarithm of the concentration of the N protein was observed in a range of 0.1 pg/mL to 10 ng/mL and the linear regression equation was $I = -16287.08$ to $11869.27 \log C$ ($R^2 = 0.985$, $n = 3$). The detection limit of the N protein was 69 fg/mL (S/N = 3), which is much lower than those of the previously reported methods as shown in Table 1.[9,37−41] As a label-free technique without a complicated labeling procedure, the proposed MAA/Co^{2+}-based CL immunoassay not only displayed great analytical performance with a relatively wide detection range and low detection limit but was also fast, simple, and cost-effective.

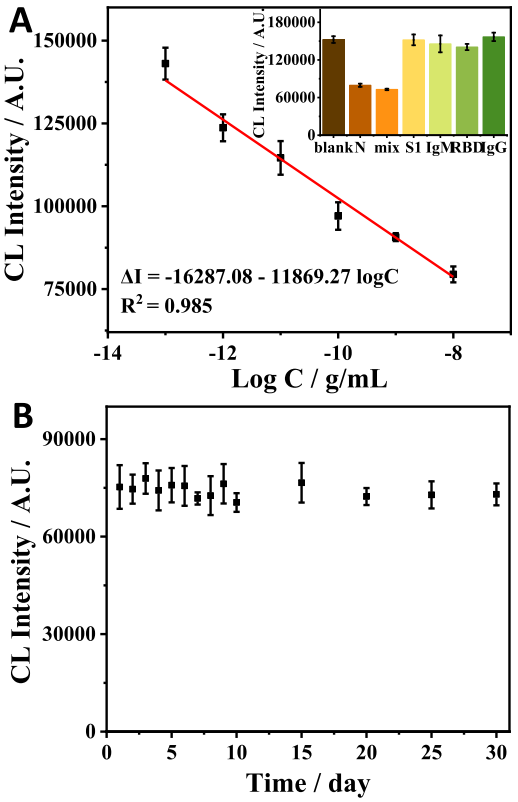

Figure 4. (A) Linear relationship between the CL response and logarithm of the N protein concentration. Reaction conditions: 50 μL of 1 mM H_2O_2 in NaOH solution (pH 12.0) was injected into 50 μL of MAA/Co^{2+}/N-Ab/BSA/N protein dispersion in a microwell. Inset: Selectivity of CL immunoassay: blank, S1 (1 ng/mL), IgM (1 ng/mL), IgG (1 ng/mL), RBD (1 ng/mL), N protein (0.1 ng/mL), and mixture (containing all of the above analytes). (B) Stability of the immunoassay.

Table 1. Comparison of the Developed CL Immunoassay with Other Reported Immunoassays for Detecting the N Protein

analytical method	linear range	detection limit	references
electrochemistry	1−1000 ng/mL	0.8 pg/mL	37
fluorescent microsphere	1−500 μg/mL	100 ng/ml	9
aptamer-assisted proximity ligation assay	50−5000 pg/mL	37.5 pg/mL	38
half-strip lateral flow assay (LFA)	0.53−0.77 ng/mL	0.65 ng/mL	39
aptamer-based salivary antigen assay employing an glucometer	1−500 pM	1.50 pM	40
labeled MB-based electrochemical assay	0.01−10 ng/mL	10 pg/mL	41
CL	0.1 pg/mL-10 ng/mL	69 fg/mL	this work

To illustrate whether or not the immunoassay could selectively determine the N protein, several interfering proteins such as IgM, S1, RBD, and IgG were chosen to check the selectivity of the immunoassay. In interference experiments, the concentration of all interfering proteins was 1 ng/mL, which was 1 order of magnitude higher than that of the N protein (0.1 ng/mL), and the mixture contained all of the interfering proteins. As can be seen in the inset of Figure 4A, the CL intensity of the N protein was obviously decreased, whereas the CL responses from interfering proteins IgM, S1, RBD, and IgG were similar to those of the blank. The CL performance of the mixture was also examined, which was close to that of the N protein, which indicated that the proposed CL immunoassay was highly selective toward the N protein by antibody−antigen recognition. Moreover, as shown in Figure 4B, the relative standard deviation (RSD) for interday detection was 2.9% in a month, indicating that the proposed immunoassay had acceptable reproducibility and reliability for detecting the N protein.

Recoveries in Clinical Samples. The clinical applicability of the as-prepared CL immunoassay was further investigated by detecting the N protein in human serum and saliva using a standard curve method. Healthy human serum samples were obtained from the First Affiliated Hospital of Nanjing Medical University and stored at −20 °C. Healthy saliva samples were collected from nonirritating whole saliva from subjects who were forbidden to eat or drink for 2 h. After centrifugation for 10 min and discarded precipitates, the supernatant was stored at −20 °C for further use. All serum samples and saliva samples were diluted properly with 0.01 M PBS (pH 7.4) prior to the measurements, and different concentrations (0.5, 1, 10, 50 pg/mL) of the N protein were added into diluted samples. As shown in Table 2, the immunoassay showed good performance with recoveries ranging from 95.7 to 102.9%, which demonstrated the applicability of the developed CL immunoassay in real samples.

Application in Clinical Samples. To test the effectiveness of MAA/Co^{2+}/N-Ab/BSA immunoassay in clinical samples

https://doi.org/10.1021/acs.analchem.1c03208
Anal. Chem. 2021, 93, 14238−14246

Table 2. Quantitative Determination of the N protein in Human Serum and Saliva Samples

sample		initial (pg/mL)	spiked (pg/mL)	measured (pg/mL)	recovery (%)
serum	1	not detected	50	47.863	95.7
	2	not detected	1	1.029	102.9
	3	not detected	0.5	0.489	97.7
saliva	1	not detected	10	10.1	101.0
	2	not detected	1	0.973	97.3

and considering the safety of the laboratory, the constructed immunoassay was coupled with an automatic CL analyzer having the magnetic separation function in the same conditions to detect the N protein in COVID-19 patient and rehabilitation patient serums. The automatic CL analyzer could detect 24 samples within 30 min, which avoids high-risk application scenarios and reduces manual operation errors. The COVID-19 patient, rehabilitation patient, and healthy human serums were collected from donors and diluted 100 times with 0.01 M PBS (pH 7.4) prior to use. The serum samples of the COVID-19 patient were used after inactivation treatment. As shown in Table 3, the concentration of the N protein in diluted serums of rehabilitation patients and COVID-19 patients were in the range of 0.21−1.96 pg/mL and 5.49−12.2 pg/mL, respectively. The concentration of the N protein in patients was higher than that in rehabilitation patients obviously. This is because only a small amount of N proteins was present in SARS-CoV-2 in the serum of rehabilitation patients. In addition, the immunoassay showed good recoveries ranging from 92.8 to 106.4%. These results demonstrate that the immunoassay could discriminate COVID-19 patients and rehabilitation patients from healthy people.

CL Quenching Mechanism of the Protein and Antigen in the Immunoassay. To elucidate the quenching mechanism of proteins in CL immunoassay, the effect of several proteins and peptides with or without cysteine (containing sulfhydryl group) incubated on the surface of MAA/Co^{2+} on the CL intensity was carried out. As shown in Figure S8, the CL intensities of MAA/Co^{2+} decreased after incubation with peptides without cysteine and increased after incubation with peptides including cysteine. All tested proteins showed the quenching effect after being assembled on MAA/Co^{2+}. Since the sulfhydryl group has an enhancement effect in peptides, but not in proteins, it was suggested that the sulfhydryl group was not exposed on the surface after the protein structure was formed and did not show an obvious effect on the CL intensity. Accordingly, the quenching effect may result not from some groups but whole protein. The difference in the quenching effect by different proteins modified on MAA/Co^{2+} may be related to the type and number of amino acid residues and spatial configurations of proteins. The CL quenching effect of proteins is proposed due to the following reasons: First, the catalytic sites of Co^{2+} were blocked by antibody proteins, leading to a decrease in the CL intensity;[28] second, proteins combined on the surface of MAA/Co^{2+} hindered the diffusion of H_2O_2 solution to a certain extent, leading to a decrease in the CL intensity;[29] and third, the influence of complex interactions of chemical groups.[42]

In the immunoassay, the binding of the N protein with much low concentration caused a much strong decrease after the immunoreaction. The immunoassay showed a good linear correlation between the CL response and the logarithm of the concentration of the N protein. To elucidate the quenching mechanism of the N protein, additional experiments were carried out. First, MAA/Co^{2+} was incubated directly with 1% BSA without the addition of the N protein antibody and then with different concentrations of N proteins. As shown in Figure S9, the CL intensities of MAA/Co^{2+}/BSA after incubating with different concentrations of N proteins were almost the same as that of the blank, indicating that N proteins could not be connected to BSA. Besides, when other proteins instead of the N protein were used for the immunoassay, the CL responses from other proteins were similar to the blank as shown in the inset of Figure 4A. These indicated that the antigen and antibody could only be specifically recognized through the antigen−antibody interaction in the immunoassay.

Furthermore, to find reasons for the decrease of the CL intensity after the antigen−antibody interaction, the microscopic bright-field images and TEM images of MAA/Co^{2+}/N-Ab/BSA as well as corresponding dynamic light scattering in the same conditions were obtained before and after incubation with different concentrations of N proteins. As can be seen in Figures S10 and S11, MAA/Co^{2+}/N-Ab/BSA has good dispersion. After being incubated with the N protein, particles were getting more and more agglomerated with the increase of the N protein concentration. As shown in Figure S12, compared with MAA/Co^{2+}/N-Ab/BSA, the light scattering intensities of the MAA/Co^{2+}/N-Ab/BSA/N protein increased with the increasing concentration of the N protein, which also demonstrated the agglomeration after immunoreactions. Thus, it was suggested that the decrease of the CL intensity after the antigen−antibody interaction was caused by agglomeration. As anti-N protein polyclonal rabbit antibodies were used in this work, one antibody could bind to two antigen molecules, and

Table 3. Quantitative Determination of the N protein in 100-fold diluted COVID-19 Patient and Rehabilitation Patient Serum Samples

serum sample		RT-PCR result	initial (pg/mL)	spiked (pg/mL)	measured (pg/mL)	recovery (%)
rehabilitation patient	1	−[a]	1.96 ± 0.23	10	11.10 ± 0.47	92.8
	2	−[a]	0.21 ± 0.05	10	10.10 ± 0.14	98.9
	3	−[a]	0.42 ± 0.02	10	11.09 ± 0.21	106.4
COVID-19 patient	1	+	8.20 ± 0.04	10	17.18 ± 0.53	94.4
	2	+	6.76 ± 0.19	10	16.48 ± 0.83	98.3
	3	+	12.20 ± 0.26	10	21.13 ± 0.51	95.2
	4	+	9.79 ± 0.11	10	18.57 ± 0.22	93.8
	5	+	5.49 ± 0.63	10	14.78 ± 0.11	95.4

[a]RT-PCR results of rehabilitation patients were positive before recovery.

https://doi.org/10.1021/acs.analchem.1c03208
Anal. Chem. 2021, 93, 14238−14246

multiple sites on one antigen could bind to multiple antibodies conjugated to functional nanomaterials, resulting in cross-linking phenomena and particle agglomeration. The aggregation after cross-linking further blocked the catalytic sites of Co^{2+} and hindered the diffusion of H_2O_2, leading to the strong quenching effect of the CL intensity.

CONCLUSIONS

In summary, we have developed a new type of CL-functionalized magnetic nanobeads MAA/Co^{2+} under very mild conditions via two steps. MAA/Co^{2+} exhibited high CL efficiency and good magnetic properties. In response to the urgent need for rapid and accurate detection of antigens of SARS-CoV-2 in COVID-19 pandemic, MAA/Co^{2+} was used to construct a label-free immunoassay for detecting the N protein by the direct connection of antibodies against the N protein on the surface of MAA/Co^{2+} via AuNPs. Compared with other reported methods, the proposed immunoassay only requires one antibody and avoids complicated labeling procedures. It is sensitive, selective, fast, simple, and low cost. It has been successfully applied for the detection of the N protein in spiked human serum and saliva with satisfactory results. In addition, the immunoassay has been integrated with an automatic CL analyzer to detect the N protein in real clinical samples, which could discriminate the patients and rehabilitation patients from healthy people. Therefore, this work provides a new family member of CL MBs, which lays an important foundation for the construction of bioassays. The immunoassay is of great application in COVID-19 clinical diagnosis. This new easy to obtain nanomaterial and the proposed strategy can also be extended to the detection of other proteins using corresponding antibodies.

ASSOCIATED CONTENT

Supporting Information

The Supporting Information is available free of charge at https://pubs.acs.org/doi/10.1021/acs.analchem.1c03208.

Chemicals and materials; XPS analysis; measurement of ζ potentials; effect of Co^{2+} concentration on the CL response; ESR spectra of $HO^{\bullet}$ and $O_2^{\bullet-}$ spin adducts generated during the CL reaction; CL signals of MAA/Co^{2+} after modified with different kinds of proteins and peptides; TEM images and CL curves of MAA with different coverage of ABEI-AuNPs; effect of pH values, H_2O_2 concentration, and N protein incubation time for the immunoreaction on the CL intensity; CL intensities of MAA/Co^{2+}/BSA after being incubated with PBS and N proteins; microscopic bright-field images; and TEM images and dynamic light scattering intensities of MAA/Co^{2+}/N-Ab/BSA after being incubated with PBS and N proteins (PDF)

AUTHOR INFORMATION

Corresponding Authors

Tengchuan Jin − *Laboratory of structural immunology, CAS Key Laboratory of innate immunity and chronic diseases, CAS Center for Excellence in Molecular Cell Science, Division of Life Sciences and Medicine, University of Science and Technology of China, Hefei, Anhui 230027, P. R. China;* orcid.org/0000-0002-1395-188X; Email: jint@ustc.edu.cn; Fax: +86-551-63600720

Hua Cui − *CAS Key Laboratory of Soft Matter Chemistry, Collaborative Innovation Center of Chemistry for Energy Materials, Department of Chemistry, University of Science and Technology of China, Hefei, Anhui 230026, P. R. China;* orcid.org/0000-0003-4769-9464; Email: hcui@ustc.edu.cn; Fax: +86-551-63600730

Authors

Shanshan Wang − *CAS Key Laboratory of Soft Matter Chemistry, Collaborative Innovation Center of Chemistry for Energy Materials, Department of Chemistry, University of Science and Technology of China, Hefei, Anhui 230026, P. R. China*

Jiangnan Shu − *CAS Key Laboratory of Soft Matter Chemistry, Collaborative Innovation Center of Chemistry for Energy Materials, Department of Chemistry, University of Science and Technology of China, Hefei, Anhui 230026, P. R. China*

Aihua Lyu − *CAS Key Laboratory of Soft Matter Chemistry, Collaborative Innovation Center of Chemistry for Energy Materials, Department of Chemistry, University of Science and Technology of China, Hefei, Anhui 230026, P. R. China*

Xiaoxue Huang − *Laboratory of structural immunology, CAS Key Laboratory of innate immunity and chronic diseases, CAS Center for Excellence in Molecular Cell Science, Division of Life Sciences and Medicine, University of Science and Technology of China, Hefei, Anhui 230027, P. R. China*

Weihong Zeng − *Laboratory of structural immunology, CAS Key Laboratory of innate immunity and chronic diseases, CAS Center for Excellence in Molecular Cell Science, Division of Life Sciences and Medicine, University of Science and Technology of China, Hefei, Anhui 230027, P. R. China*

Complete contact information is available at: https://pubs.acs.org/10.1021/acs.analchem.1c03208

Author Contributions

All authors have given approval to the final version of the manuscript.

Notes

The authors declare no competing financial interest.

ACKNOWLEDGMENTS

This research was supported by a COVID-19 special task grant by the Chinese Academy of Sciences Clinical Research Hospital (Hefei) with Grant Nos. YD2060002008 and YD2070002017. The support of this research by the National Key Research and Development Program of China (Grant No. 2016YFA0201300) are gratefully acknowledged.

REFERENCES

(1) Wang, C.; Horby, P. W.; Hayden, F. G.; Gao, G. F. *The Lancet* **2020**, *395*, 470−473.

(2) Chan, J. F.-W.; Yuan, S.; Kok, K.-H.; To, K. K.-W.; Chu, H.; Yang, J.; Xing, F.; Liu, J.; Yip, C. C.-Y.; Poon, R. W.-S.; Tsoi, H.-W.; Lo, S. K.-F.; Chan, K.-H.; Poon, V. K.-M.; Chan, W.-M.; Ip, J. D.; Cai, J.-P.; Cheng, V. C.-C.; Chen, H.; Hui, C. K.-M.; Yuen, K.-Y. *The Lancet* **2020**, *395*, 514−523.

(3) ⟨WHO-2019-nCoV-Antigen Detection-2020.1-eng.pdf⟩.

(4) Zhu, Z.; Liu, G.; Meng, K.; Yang, L.; Liu, D.; Meng, G. *Genome Biol. Evol.* **2021**, *13*, No. evab015.

(5) Zhao, H.; Liu, F.; Xie, W.; Zhou, T. C.; OuYang, J.; Jin, L.; Li, H.; Zhao, C. Y.; Zhang, L.; Wei, J.; Zhang, Y. P.; Li, C. P. *Sens. Actuators, B* **2021**, *327*, No. 128899.

(6) Kasetsirikul, S.; Umer, M.; Soda, N.; Sreejith, K. R.; Shiddiky, M. J. A.; Nguyen, N. T. *Analyst* **2020**, *145*, 7680−7686.
(7) Liu, D.; Ju, C.; Han, C.; Shi, R.; Chen, X.; Duan, D.; Yan, J.; Yan, X. *Biosens. Bioelectron.* **2020**, *173*, No. 112817.
(8) Seo, G.; Lee, G.; Kim, M. J.; Baek, S. H.; Choi, M.; Ku, K. B.; Lee, C. S.; Jun, S.; Park, D.; Kim, H. G.; Kim, S. J.; Lee, J. O.; Kim, B. T.; Park, E. C.; Kim, S. I. *ACS Nano* **2020**, *14*, 5135−5142.
(9) Zhang, C.; Zhou, L.; Du, K.; Zhang, Y.; Wang, J.; Chen, L.; Lyu, Y.; Li, J.; Liu, H.; Huo, J.; Li, F.; Wang, J.; Sang, P.; Lin, S.; Xiao, Y.; Zhang, K.; He, K. *Front. Cell. Infect. Microbiol.* **2020**, *10*, No. 553837.
(10) Li, D.; Li, J. *J. Clin. Microbiol.* **2020**, *59*, No. e02160.
(11) Padoan, A.; Cosma, C.; Sciacovelli, L.; Faggian, D.; Plebani, M. *Clin. Chem. Lab. Med.* **2020**, *58*, 1081−1088.
(12) Li, Y.; Hu, X.; Tu, Y.; Wu, T.; Wang, B.; Ma, H.; Zeng, W.; Zhao, D.; Mengist, H. M.; Kombe, A. J. K.; Zheng, M.; Xu, Y.; Jin, T. *Front Public Health* **2020**, *8*, No. 339.
(13) Liu, H.; Dai, E.; Xiao, R.; Zhou, Z.; Zhang, M.; Bai, Z.; Shao, Y.; Qi, K.; Tu, J.; Wang, C.; Wang, S. *Sens. Actuators, B* **2021**, *329*, No. 129196.
(14) Yakoh, A.; Pimpitak, U.; Rengpipat, S.; Hirankarn, N.; Chailapakul, O.; Chaiyo, S. *Biosens. Bioelectron.* **2021**, *176*, No. 112912.
(15) Gambino, C. M.; Lo Sasso, B.; Colomba, C.; Giglio, R. V.; Agnello, L.; Bivona, G.; Ciaccio, M. *Biochem. Med.* **2020**, *30*, No. 030901.
(16) Ma, H.; Zeng, W.; He, H.; Zhao, D.; Jiang, D.; Zhou, P.; Cheng, L.; Li, Y.; Ma, X.; Jin, T. *Cell. Mol. Immunol.* **2020**, *17*, 773−775.
(17) Mekonnen, D.; Mengist, H. M.; Derbie, A.; Nibret, E.; Munshea, A.; He, H.; Li, B.; Jin, T. *Rev. Med. Virol.* **2020**, *31*, No. e2181.
(18) Deng, J. Q.; Tian, F.; Liu, C.; Liu, Y.; Zhao, S.; Fu, T.; Sun, J. S.; Tan, W. H. *J. Am. Chem. Soc.* **2021**, *143*, 7261−7266.
(19) Sabbih, G. O.; Korsah, M. A.; Jeevanandam, J.; Danquah, M. K. *Biotechnol. Prog.* **2020**, *37*, No. e3096.
(20) Zeng, W.; Ma, H.; Ding, C.; Yang, Y.; Sun, Y.; Huang, X.; He, W.; Xiang, Y.; Gao, Y.; Jin, T. *Signal Transduct Target Ther.* **2021**, *6*, No. 35.
(21) Radi, Abd-Elgawad.; Munoz-Berbel, Xavier.; Lates, Vasilica.; Martyc, Jean-Louis. *Biosens. Bioelectron.* **2009**, *24*, 1888−1892.
(22) Liu, D.; Huang, G.; Yu, Y.; He, Y.; Zhang, H.; Cui, H. *Chem. Commun.* **2013**, *49*, 9794−9796.
(23) Huang, Y.; Gao, L.; Cui, H. *ACS Appl. Mater. Interfaces* **2018**, *10*, 17040−17046.
(24) Chen, H.; Lin, L.; Li, H.; Lin, J. *Coord. Chem. Rev.* **2014**, *263*−*264*, 86−100.
(25) Mao, X.; Lu, Y.; Zhang, X.; Huang, Y. *Talanta* **2018**, *188*, 161−167.
(26) Qin, G.; Zhao, S.; Huang, Y.; Jiang, J.; Ye, F. *Anal. Chem.* **2012**, *84*, 2708−2712.
(27) Li, Y.; Ji, X.; Liu, B. *Anal. Bioanal. Chem.* **2011**, *401*, 213−219.
(28) Kong, W.; Zhao, X.; Zhu, Q.; Gao, L.; Cui, H. *Anal. Chem.* **2017**, *89*, 7145−7151.
(29) Yang, R.; Li, F.; Zhang, W.; Shen, W.; Yang, D.; Bian, Z.; Cui, H. *Anal. Chem.* **2019**, *91*, 13006−13013.
(30) Wang, C.; Wang, J.; Li, M.; Qu, X.; Zhang, K.; Rong, Z.; Xiao, R.; Wang, S. *Analyst* **2016**, *141*, 6226−6238.
(31) Tian, D.; Zhang, H.; Chai, Y.; Cui, H. *Chem. Commun.* **2011**, *47*, 4959−4961.
(32) Burdo, T. G. S.; W, R. *Anal. Chem.* **1975**, *47*, 1639.
(33) Liu, M.; Zhang, H.; Shu, J.; Liu, X.; Li, F.; Cui, H. *Anal. Chem.* **2014**, *86*, 2857−2861.
(34) Liu, Y.; Shen, W.; Cui, H. *Anal. Chem.* **2019**, *91*, 10614−10621.
(35) Chai, Y.; T, D.; Wang, W.; Cui, H. *Chem. Commun.* **2010**, *46*, 7560−7562.
(36) Cao, J. T.; Zhang, W. S.; Wang, H.; Ma, S. H.; Liu, Y. M. *Spectrochim. Acta, Part A* **2019**, *219*, 281−287.
(37) Eissa, S.; Zourob, M. *Anal. Chem.* **2021**, *93*, 1826−1833.
(38) Liu, R.; He, L.; Hu, Y.; Luo, Z.; Zhang, J. *Chem. Sci.* **2020**, *11*, 12157−12164.
(39) Grant, B. D.; Anderson, C. E.; Williford, J. R.; Alonzo, L. F.; Glukhova, V. A.; Boyle, D. S.; Weigl, B. H.; Nichols, K. P. *Anal. Chem.* **2020**, *92*, 11305−11309.
(40) Singh, N. K.; Ray, P.; Carlin, A. F.; Magallanes, C.; Morgan, S. C.; Laurent, L. C.; Aronoff-Spencer, E. S.; Hall, D. A. *Biosens. Bioelectron.* **2021**, *180*, No. 113111.
(41) Li, J.; Lillehoj, P. B. *ACS Sens.* **2021**, *6*, 1270−1278.
(42) Zhang, Z. F.; Cui, H.; Lai, C. Z.; Liu, L. J. *Anal. Chem.* **2005**, *77*, 3324−3329.

https://doi.org/10.1021/acs.analchem.1c03208
Anal. Chem. 2021, 93, 14238−14246